Order-*N* first-principles calculation method for self-consistent ground-state electronic structures of semi-infinite systems

Takashi Sasaki, Tomoya Ono, and Kikuji Hirose
Department of Precision Science and Technology, Osaka University, Suita, Osaka 565-0871, Japan
(Received 14 June 2006; published 15 November 2006)

We present an efficient and highly accurate first-principles calculation method with linear system-size scaling to determine the self-consistent ground-state electron-charge densities of nanostructures suspended between semi-infinite bulks by directly minimizing the energy functional. By making efficient use of the advantages of the real-space finite-difference method, we can impose arbitrary boundary conditions on models and employ spatially localized orbitals. These advantages enable us to calculate the ground-state electron-charge densities in semi-infinite systems. Examples of electronic structure calculations for a one-dimensional case and a conductance calculation for sodium nanowires are presented. The calculated electronic structure of the one-dimensional system agrees well with the exact analytical solution, and the conduction properties of the sodium nanowires are consistent with experimental and other theoretical results. These results imply that our procedure enables us to accurately compute self-consistent electronic structures of semi-infinite systems.

DOI: 10.1103/PhysRevE.74.056704 PACS number(s): 05.10.−a, 73.20.−r, 73.63.Rt, 73.22.−f

I. INTRODUCTION

The desire to continue the current trend of the miniaturization of electronic devices coupled with the evolution of new techniques for nanoscale modification has opened up the possibility of fabricating nanoscale devices [1]. A number of possible short- and long-term semiconductor device technologies rely on abrupt metal-semiconductor or metal-insulator contacts with nanometer dimensions and/or internal nanoscale inhomogeneity. When predicting the properties of these nanoscale devices, the electronic structures of a few atomic layers near the surface or interface are crucial. Additionally, in the last decade, nanoscale wires [2] have attracted considerable attention because they are expected to be some of the fundamental components of nanoscale electronic devices. The understanding of the electronic structures and the electron-conduction properties of nanostructures suspended between semi-infinite bulks in such situations is an extremely active research topic at present.

The first-principles electronic structure calculation is today an essential tool for investigating the physics and chemistry of nanostructures. An important reason for the success of this technique is the development of the density functional theory (DFT) [3]. The advantage of the first-principles DFT over more empirical approaches is the high accuracy and robustness of the technique, which does not depend on empirical parameters determined by fitting experimental data or on *ad hoc* assumptions. For the strict and detailed theoretical predictions of the electronic structures of a system in which nanostructures are connected to semi-infinite bulks, the elimination of artifacts and accurate modeling of the system are indispensable. Prevailing calculations aiming to simulate such systems have in most cases suffered from several drawbacks. One of the most common approaches with a plane-wave basis set uses artificial periodic slab models in place of semi-infinite bulks. To overcome this difficulty, two types of procedures have been proposed so far: solving the Lippmann-Schwinger equation with jellium electrodes [4,5] and constructing the electronic structure via Green's functions instead of using eigenstates [6]. The jellium model, homogeneous electron gas, lacks the minimum atomic detail that is crucial for examining interactions between surfaces and objective nanostructures. In addition, although the Green's function methods can treat crystalline bulks, the computational effort to calculate the Green's functions is proportional to N^2 [7], where N is the number of atoms in the system.

Here, we present an approach that is free from these problems. Our procedure is based on the real-space finite-difference (RSFD) method [8–16] and the direct minimization [17] of the energy functional proposed by Mauri, Galli, and Car (MGC) [18]. The RSFD methods allow us to impose arbitrary boundary conditions on models and to introduce spatially localized orbitals easily. By combining the RSFD method with the MGC energy functional, the *self-consistent* ground-state electron-charge densities of nanostructures attached to semi-infinite crystalline bulks can be obtained satisfactorily [17]. In addition, since a system is assumed to be described in terms of localized orbitals, this procedure makes it possible to perform calculations with linear system-size scaling, i.e., order-*N* calculations. To demonstrate the general applicability of this method, the calculations of the ground-state electron-charge densities of nanostructures suspended between semi-infinite crystalline bulks are presented.

The rest of the paper is organized as follows. In Sec. II, we give in detail the first-principles computation scheme for nanostructures with semi-infinite systems. In Sec. III, we present two test calculations to demonstrate the general applicability of our procedure for semi-infinite systems: one-dimensional case in which a constant potential is sandwiched between infinitely continuing periodic square-well potentials, and the electronic structure calculations of Na nanowires connected to semi-infinite crystalline bulks. In Sec. IV, we summarize and give an outlook of our future work.

II. THEORETICAL FORMALISM

A. Direct minimization of MGC energy functional

The correct self-consistent ground-state solution of the self-consistent Kohn-Sham equation is derived as output quantities by the direct minimization of the MGC energy functional [18], which is identical to the standard energy functional of DFT [17]. This energy functional is given by

$$E[Q,\{\phi\}] = 2\left(\sum_{i,j}^{M} Q_{ij}\left\langle \phi_i\left| -\frac{1}{2}\nabla^2 \right| \phi_j\right\rangle + F[\rho]\right) + \eta\left\{N_{\mathrm{ele}} - \int \rho(\boldsymbol{r})d\boldsymbol{r}\right\}, \quad (1)$$

where $\{\phi_i\}$ is an arbitrary set of M linearly independent overlapping wave functions, $F[\rho]$ is the sum of the Hartree, ionic, exchange-correlation, and external potential energy functionals, η is a Lagrange multiplier introduced to adjust the number of electrons in the system, N_{ele} is the number of electrons in the system, and Q is the first-order expansion of the inverse of the overlap matrix $Q=2I-S$, where S is the overlap matrix $S_{ij}=\langle\phi_i|\phi_j\rangle$ and I is the identity matrix. For simplicity, we assume that $\{\phi_i\}$ is a set of real functions and the spin degrees of freedom are compensated. The electron-charge density and the total charge of the system are defined as

$$\rho(\boldsymbol{r}) = \rho[Q,\{\phi\}](\boldsymbol{r}) = 2\sum_{i,j}^{M} Q_{ij}\phi_j(\boldsymbol{r})\phi_i(\boldsymbol{r}), \quad (2)$$

and $\Sigma_{i,j}^{M} 2Q_{ij}S_{ij}$, respectively. $E[Q,\{\phi\}]$ is minimized using a steepest-descent or conjugate-gradient algorithm without the constraint of the orthonormalization of wave functions.

B. Real-space finite-difference method

The MGC energy functional is minimized based on the RSFD approach [8–16]. In this approach, we perform electronic structure calculations without the explicit use of a basis. We impose a simple, uniform orthogonal three-dimensional grid on the system where the points are described in a finite domain by (x_i, y_j, z_k). The wave function and the potential are put on the grid. Derivatives arising from the kinetic energy operator are approximated by the finite-difference formula. In contrast to methods which use a plane-wave basis, the RSFD calculations are performed completely in real space without forced periodic boundary conditions. Therefore, we can employ arbitrary boundary conditions and introduce spatially localized orbitals to realize the electronic structure calculations for semi-infinite systems.

C. Localized orbitals

The form of the energy functional of Eq. (1) is introduced for the computation with linear system-size scaling, and each wave function ϕ can be replaced by a Wannier-like function (i.e., a localized orbital which has nonzero components only inside a given localization region) to reduce computational efforts. The minimization of E with respect to *localized orbitals* leads to a variety of minima if the number of orbitals is taken to be equal to the number of occupied states or the radius of localized orbitals R_{LO} is too small, although the minimization of the functional E with respect to *extended orbitals* can be easily performed without being trapped at metastable configurations [17]. The inclusion of extra orbitals $(M>N_{\mathrm{ele}}/2)$ overcomes the multiple minima problem [19]. R_{LO} is also the parameter that controls the accuracy of the calculation. The number of localized orbitals M and R_{LO} are set to be large enough to obtain the desired accuracy.

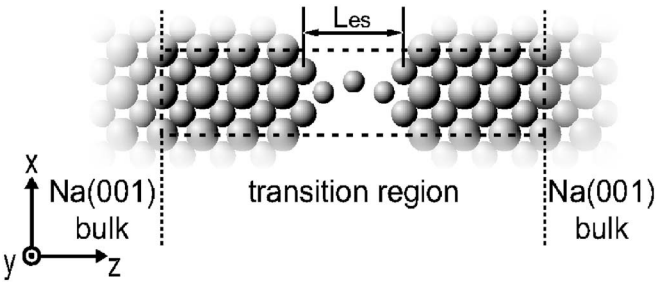

FIG. 1. Schematic representation of computational model in which the three-sodium-atom nanowire is connected to Na(001) semi-infinite crystalline bulks. The rectangle enclosed by broken lines represents the supercell used for the conductance calculation. L_{es} is the electrode spacing which corresponds to the distance between the top atomic layers of the electrodes.

D. Extension to semi-infinite systems

Let us consider the procedure for obtaining the self-consistent Kohn-Sham ground-state electron-charge densities for a nanostructure attached to semi-infinitely continuing crystalline bulks (see, Fig. 1, for an example). The transition region composed of objective nanostructures is representative of, for example, a nanoscale junction, a tunnel junction in a tip-sample system (e.g., a scanning tunneling microscope), an interface between different bulks, an interstitial lattice defect or disorder, and so on. Here, two-dimensional periodicity is assumed in the x and y directions and nonperiodicity in the z direction. The use of the RSFD method and localized orbitals can reduce the computational effort to have a linear system-size scaling and enables us to explicitly divide orbitals into two types: orbitals localized only in the bulk regions and orbitals extending within the transition region.

The computational scheme consists of two main steps. (i) Localized orbitals and potentials in the bulk regions are determined using the three-dimensional periodic supercell technique. During the minimization of the MGC energy functional of Eq. (1), η is adjusted to give the correct number of electrons. (ii) To obtain the ground-state electronic structure in the transition region, only the orbitals extending within the transition region are optimized, with the chemical potential η fixed at the value obtained in step (i). The semi-infinite crystalline bulks are regarded as reservoirs or receivers of electrons. For the minimization, there remains a requirement of matching the effective potential inside the transition region with those in the bulk regions at the boundaries. To deal with the semi-infinite boundary conditions for the potential, we

make a simple observation that the sum of the Hartree and ionic potentials, $v(\boldsymbol{r})$, deep inside a solid surface is very close to the corresponding bulk potential. This fact leads to a reasonable approximation which forms a natural boundary condition for semi-infinite systems:

$$v(\boldsymbol{r}) = \begin{cases} v_{l,\mathrm{bulk}}(\boldsymbol{r}), & z \leqq z_0, \\ v_{\mathrm{trans}}(\boldsymbol{r}), & z_1 < z < z_{N_z}, \\ v_{r,\mathrm{bulk}}(\boldsymbol{r}), & z \geqq z_{N_z+1}, \end{cases} \tag{3}$$

where $v_{l,\mathrm{bulk}}(\boldsymbol{r})$, $v_{\mathrm{trans}}(\boldsymbol{r})$ and $v_{r,\mathrm{bulk}}(\boldsymbol{r})$ are the potentials of the left bulk, transition region, and right bulk, respectively. The plane $z=z_0$ ($z=z_{N_{z+1}}$) is the right (left) limit of the left (right) bulk region. The transition region should be large enough so that the potentials on these boundary planes are sufficiently close to those of the bulks such that Eq. (3) holds.

$v(\boldsymbol{r})$ is computed using the Poisson equation under the nonperiodic boundary condition in the z direction and periodic boundary conditions in the x and y directions,

$$\nabla^2 v(\boldsymbol{r}) = -4\pi[\rho_{\mathrm{nuc}}(\boldsymbol{r}) + \rho(\boldsymbol{r})] \tag{4}$$

with $\rho_{\mathrm{nuc}}(\boldsymbol{r})$ being the charge density of the ions. To satisfy Eq. (3) in the framework of the RSFD method, the following processes are carried out: Equation (4) is discretized on the grid points using a matrix formalism coupled to the finite-difference method,

$$\begin{pmatrix} D_{xy}-2C_z & C_z & 0 & \cdots & 0 \\ C_z & D_{xy}-2C_z & \ddots & & \vdots \\ 0 & \ddots & \ddots & \ddots & 0 \\ 0 & & \ddots & D_{xy}-2C_z & C_z \\ 0 & \cdots & 0 & C_z & D_{xy}-2C_z \end{pmatrix} \times \begin{pmatrix} v_{xy}(z_1) \\ v_{xy}(z_2) \\ \vdots \\ v_{xy}(z_{N_z-1}) \\ v_{xy}(z_{N_z}) \end{pmatrix} = -4\pi \begin{pmatrix} P_{xy}(z_1) - C_z v_{xy}(z_0) \\ P_{xy}(z_2) \\ \vdots \\ P_{xy}(z_{N_z-1}) \\ P_{xy}(z_{N_z}) - C_z v_{xy}(z_{N_{z+1}}) \end{pmatrix}, \tag{5}$$

where D_{xy} is an $(N_x \times N_y)$-dimensional matrix representing the second-order derivative in the x and y directions [13], $v_{xy}(z_k)[P_{xy}(z_k)]$ is a columnar vector consisting of $N_x \times N_y$ values of $v(\boldsymbol{r})[\rho_{nuc}(\boldsymbol{r})+\rho(\boldsymbol{r})]$ on the x-y plane at $z=z_k$ and C_z is a constant matrix proportional to the $(N_x \times N_y)$-dimensional unit matrix I_{xy} [11], i.e.,

$$C_z = \frac{1}{h_z^2} I_{xy}, \tag{6}$$

where h_z is the grid spacing in the z direction, and N_x, N_y, and N_z are the numbers of grid points in the x, y, and z directions, respectively. Here, we employed the central finite-difference formula for the second-order derivative. To set up the simultaneous equations of Eq. (5), the boundary values of $v_{xy}(z_0)$ and $v_{xy}(z_{N_z+1})$ are required, for which we adopt the potential $v(\boldsymbol{r})$ at the boundaries of the bulk regions calculated in step (i). These simultaneous equations are solved using a steepest-descent or conjugate-gradient algorithm. Note that the electron charge density automatically becomes continuous at the boundaries between the bulk and transition regions by minimizing the energy functional, while the boundary condition is imposed on the potential.

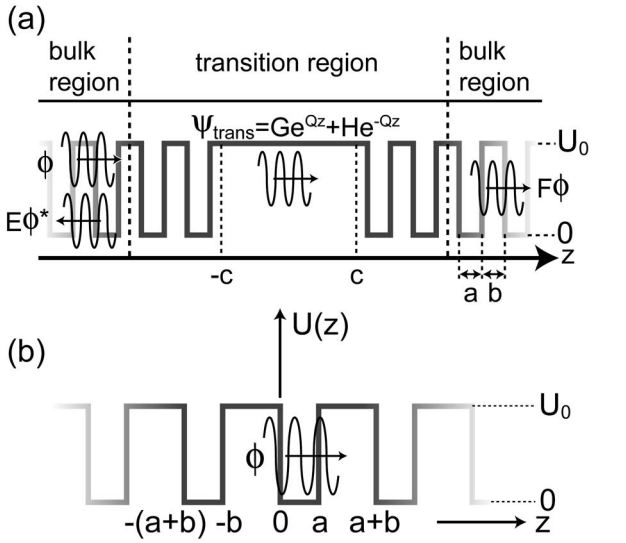

FIG. 2. (a) Schematic representation of one-dimensional system with transition region between left and right bulks. The potential in the transition region is composed of a constant potential between two square-well potentials, and the potentials in the bulk regions are infinitely continuing periodic square-well ones. The units are atomic units. (b) Square-well periodic potential model, introduced by Kronig and Penney [20]. Parameters a, b, c, and U_0 are set to be 1.0, 1.0, 3.0, and 3.0, respectively.

III. APPLICATION

A. One-dimensional system

To test the applicability of our method for the calculation for electronic structures of semi-infinite systems, we consider the one-dimensional system shown in Fig. 2(a), in which a constant potential is sandwiched between infinitely continuing periodic square-well potentials with a barrier height of U_0. The wave functions for this simple system can be solved in terms of elementary functions. Note that the solutions of the wave functions in the bulk regions $\phi(z)$ of Fig. 2(b) are analytical, as introduced by Kronig and Penney [20] and Kittel [21]. In the regions within the barrier and valley, these analytical solutions for the waves with energy ϵ are of the forms

$$\phi_b(z) = Ae^{\sqrt{2U_0-2\epsilon}z} + Be^{-\sqrt{2U_0-2\epsilon}z}, \tag{7}$$

and

$$\phi_v(z) = Ce^{i\sqrt{2\epsilon}z} + De^{-i\sqrt{2\epsilon}z}, \tag{8}$$

respectively. The constants A, B, C, and D are determined by solving the simultaneous equations

$$\begin{pmatrix} 1 & 1 & -1 & -1 \\ \sqrt{U_0-\epsilon} & -\sqrt{U_0-\epsilon} & -i\sqrt{\epsilon} & i\sqrt{\epsilon} \\ e^{\sqrt{2U_0-2\epsilon}a} & e^{-\sqrt{2U_0-2\epsilon}a} & -e^{-i\sqrt{2\epsilon}b+ik(a+b)} & -e^{i\sqrt{2\epsilon}b+ik(a+b)} \\ \sqrt{U_0-\epsilon}e^{\sqrt{2U_0-2\epsilon}a} & -\sqrt{U_0-\epsilon}e^{-\sqrt{2U_0-2\epsilon}a} & -i\sqrt{\epsilon}e^{-i\sqrt{2\epsilon}b+ik(a+b)} & i\sqrt{\epsilon}e^{i\sqrt{2\epsilon}b+ik(a+b)} \end{pmatrix} \begin{pmatrix} A \\ B \\ C \\ D \end{pmatrix} = 0 \tag{9}$$

with the constraint that the determinant of the matrix consisting of the coefficients of A, B, C, and D vanishes.

The wave function in the transition region $\psi_{\text{trans}}(z)$ is described by a linear combination of exponential functions.

$$\psi_{\text{trans}}(z) = Ge^{\sqrt{2U_0-2\epsilon}z} + He^{-\sqrt{2U_0-2\epsilon}z}. \tag{10}$$

The coefficients are determined by solving the simultaneous equations derived from the conventional wave-function matching procedure [Fig. 2(a)] so that the wave functions and the first-order derivatives of the wave functions are continuous at $z=-c$ and $z=c$, i.e.,

$$\phi_b(-c) + E\phi_b^*(-c) = Ge^{-\sqrt{2U_0-2\epsilon}a} + He^{\sqrt{2U_0-2\epsilon}c}, \tag{11}$$

$$\phi_b'(-c) + E\phi_b^{*\prime}(-c) = \sqrt{2U_0-2\epsilon}(Ge^{-\sqrt{2U_0-2\epsilon}c} - He^{\sqrt{2U_0-2\epsilon}c}), \tag{12}$$

$$F\phi_b(c) = Ge^{\sqrt{2U_0-2\epsilon}c} + He^{-\sqrt{2U_0-2\epsilon}c}, \tag{13}$$

$$F\phi_b'(c) = \sqrt{2U_0-2\epsilon}(Ge^{\sqrt{2U_0-2\epsilon}c} - He^{-\sqrt{2U_0-2\epsilon}c}), \tag{14}$$

where $\phi_b'(z)$ is the first-order derivative of the wave function $\phi_b(z)$ with respect to the z direction. In this test, incident wave functions incoming from one side $\phi(z)$, reflecting to the side $E\phi^*(z)$ and transmitting to the other side $F\phi(z)$ are sampled using a regularly spaced set of 60 k points in the irreducible Brillouin zone for the analytical solution of the square potential. In the calculation of the present procedure, a potential consisting of 60 wells is employed to set up the localized orbitals, the number of which is 180 in the bulk regions. Localized orbitals are placed such that their centers are at regular intervals of ~0.67 a.u. $[60\times(a+b)/180]$. During the optimization of the charge density of the transition region, the number of localized orbitals in the region is chosen to be 21 with their intervals being ~0.67 a.u. The total number of localized orbitals is $M=381$. We regard an orbital whose center is in one region (bulk region or transition region) as belonging to the region. In the process of obtaining the ground-state electronic structure in the transition region, only the orbitals belonging to the transition region are optimized. The grid spacing h_z is taken to be 0.1 a.u. and η is 1.75 a.u., which is taken such that the total charge per well is 2.0 electrons.

Electron-charge densities obtained by the analytical procedures and present method are shown in Fig. 3. The computed charge densities asymptotically approach the analytical solution as R_{LO} becomes large. When R_{LO} is 5.0 a.u., the relative error of the number of electrons in the transition region is $<0.06\%$. Thus, our calculation method reproduces well the ground-state electron-charge density of a nanostructure attached to semi-infinite bulks.

B. Atomic nanowire

Free-standing atomic nanowires, with cross sections as small as a few square nanometers, can now be fabricated using several recently developed experimental techniques [22–25]. Among the many exciting discoveries about these atomic-scale objects is the observed conductance quantization at elevated temperatures, including room temperature. It has been demonstrated that monatomic nanowires made of monovalent atoms such as Na, K, and Au have a strong tendency toward quantized conductance in the unit of $G_0(=2e^2/h)$, and the conductance is stable when the wire is stretched [23,24,26,27], where e is the electron-charge and h is Planck's constant. To obtain accurate theoretical knowledge of electron-conduction properties, it is essential to calculate the self-consistent ground-state electronic structures of the nanowire in contact with two truly semi-infinite crystalline electrodes. In the following, we apply our formalism to the investigation of the relationship between the optimized geometry and electric conductance of a three-sodium-atom nanowire suspended between two semi-infinite crystalline electrodes during its elongation.

1. Atomic geometry

We first determine the optimized atomic geometries of the three-sodium-atom nanowire suspended between crystalline electrodes during its elongation by employing a standard supercell technique with a three-dimensional periodic boundary. The supercell contains the three-atom nanowire and four atomic layers of electrodes on each side. The distance between the (001) atom plane of electrode surface and the edge atom of the three-atom nanowire is chosen to be $a_0/2$, where a_0 (=8.1048 a.u.) is the lattice constant of Na bulk. The grid spacing is taken to be ~0.675 a.u., which corresponds to a cutoff energy of ~21.34 Ry in the conventional plane-wave approach. The exchange-correlation interaction between electrons is treated using the local density approximation [28] within the framework of DFT [3]. The norm-conserving pseudopotentials of Toullier-Martins [29,30] are used to describe the electron-ion interaction. We employ the nine-point finite-difference formula, i.e., the case of $N=4$ in Ref. [9], for the derivative arising from the kinetic-energy operator. As an initial configuration at $L_{es}=20.26$ a.u., the center atom is randomly located in the nanowire and is relaxed through the optimization, where L_{es} is the electrode spacing which corresponds to the distance between the top atomic layers of

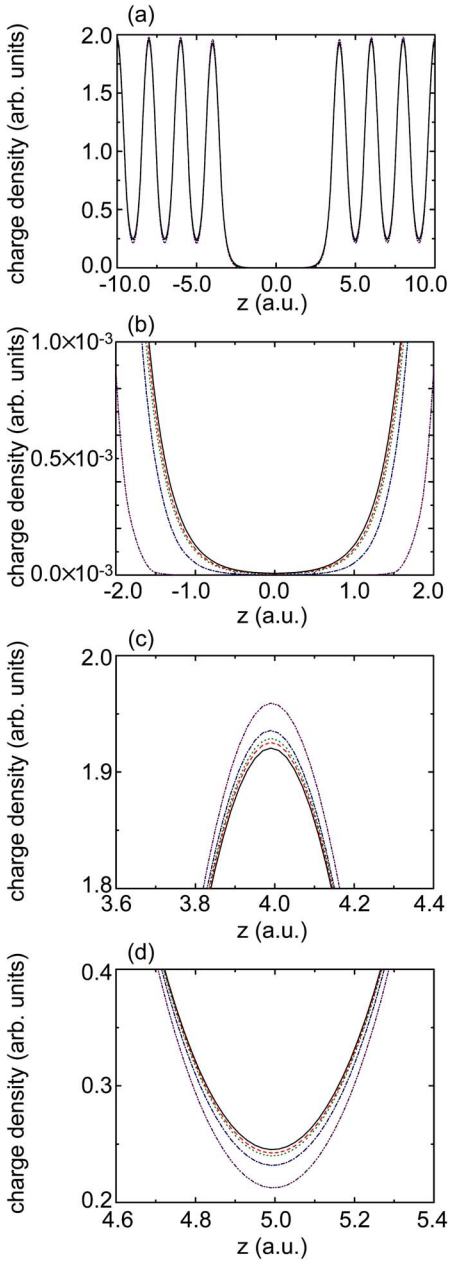

FIG. 3. (Color online) Comparison of electron-charge densities obtained by the analytical procedure and present method. For the analytical solution, the sum of the densities in the cases of right-going and left-going incident waves is depicted. The black solid curve is the exact analytical solution. The broken (red) curve, dotted (green) curve, chain (blue) curve and chain double-dashed (purple) curve represent the results of our procedure where the localization radii R_{LO} are 5.0, 4.0, 3.0, and 2.0 a.u., respectively. (b)–(d) are enlargements of the interesting parts of (a).

the electrodes. Then, we stretched the nanowire in steps of $\Delta L_{es} \sim 0.675$ a.u. and relieved the force on the atom repetitiously. The position of the center atom in the nanowire is optimized while the other atoms are fixed during the stretching process. The nanowire exhibits a bent structure at first. When elongated up to $L_{es}=21.61$ a.u., the nanowire manifests a geometrical transition from a bent structure to a straight structure, and finally brakes at $L_{es}=23.64$ a.u.

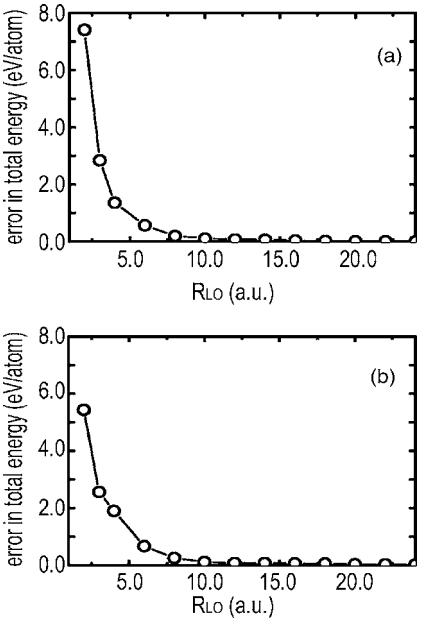

FIG. 4. Convergence of error in total energy as a function of R_{LO} in [001] direction for (a) Na bulk and direction parallel to wire axis for (b) infinite single-row Na wire.

2. Electronic structure and conductance

Next, the electronic structure and conductance of the nanowires are evaluated using the atomic geometries obtained in the preceding subsection. The transition region is chosen to be the area between the vertical dotted lines in Fig. 1, which includes the three-atom nanowire and the eight atomic layers of electrodes on each side so that the potentials at both boundaries in the transition region can be smoothly connected to the bulklike potentials inside the crystalline electrodes, and thus the number of atoms in the region is 63. A grid spacing of ~ 0.675 a.u. is employed. To reduce the computational effort, the local pseudopotentials introduced by Hamann *et al.* [31] are adopted to describe the electron-ion interaction. The extension of the methodology to the case of nonlocal pseudopotentials is straightforward. We employ the three-point finite-difference formula for the derivative arising from the kinetic-energy operator, which is in the case of $N=1$ in Ref. [9]. The localization radius R_{LO} is a parameter controlling the accuracy of calculations. In Fig. 4, the convergences of the error in total energy as a function of R_{LO} for the Na bulk and the infinite single-row Na wire are shown. The orbitals are localized only in the [001] direction for the Na bulk and in the direction parallel to the wire axis for the infinite single-row wire, whereas the orbitals are not localized in the other directions. To avoid serious errors in the total energies due to the local minima problem, R_{LO} is set to be 10.0 a.u. [32] and the number of localized orbitals in transition region is chosen to be 63 and the total number of localized orbitals is $M=175$ for $N_{\mathrm{ele}}=175$. The orbitals are localized only in the [001] direction in the same way as the cases of the Na bulk and infinite single-row wire.

We then evaluate the self-consistent electronic structures of the nanowires suspended between the semi-infinite crystalline electrodes using the atomic geometries obtained in the

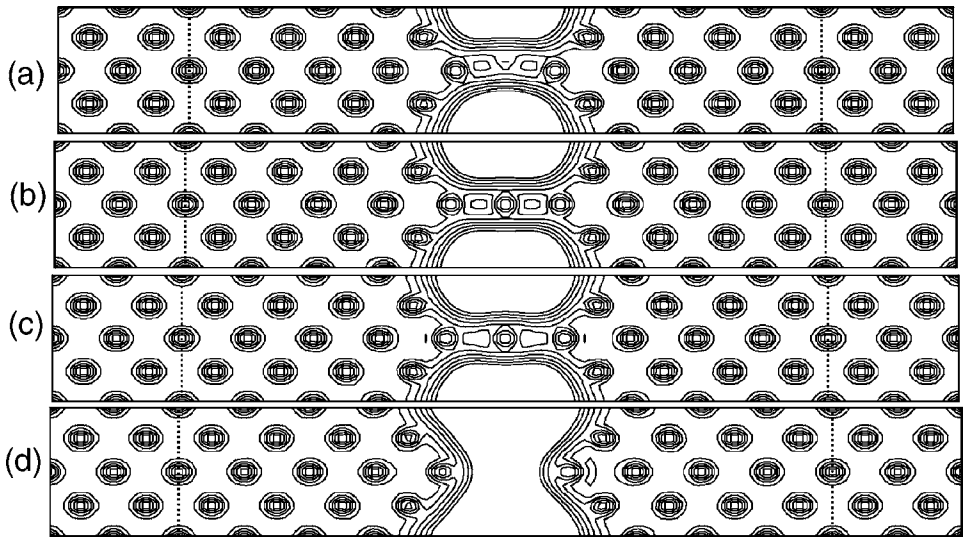

FIG. 5. Charge density contours of Na wire-bulk interface of Fig. 1. The electrode spacings L_{es} are 20.26, 21.61, 22.96, and 24.31 a.u. for (a)–(d), respectively. The vertical dotted lines represent the boundaries between the transition region and the bulk region. Each contour represents ten-sevenths or seven-tenths the density of the adjacent contour.

above step. We found that the transition region in the optimized atomic structure is electrically neutral. The charge transfer from the transition region to the electrodes is less than 0.03 electrons. Figure 5 shows the ground-state charge density distribution $\rho(\boldsymbol{r})$ along a cross section of the (110) plane for the Na nanowire in contact with the Na(001) electrodes, for which the contours of the transition region match those of the bulk region across the boundaries between them. Indeed, for all the systems we have investigated, a perfect match of charge density at the boundary is achieved by including several layers of bulk electrodes within the transition region. Because the potential is uniquely determined by the charge distribution, this nontrivial result is strong evidence that the transition region has been chosen to be large enough such that the potential is effectively screened and relaxes to the bulk value at the boundaries.

Let us discuss the electron-conduction properties of the nanowire. The global scattering wave function extending infinitely over the entire system near both boundaries of the transition region is determined using the overbridging boundary-matching formula [13,33] with the electronic structure obtained by the above-mentioned procedure. The

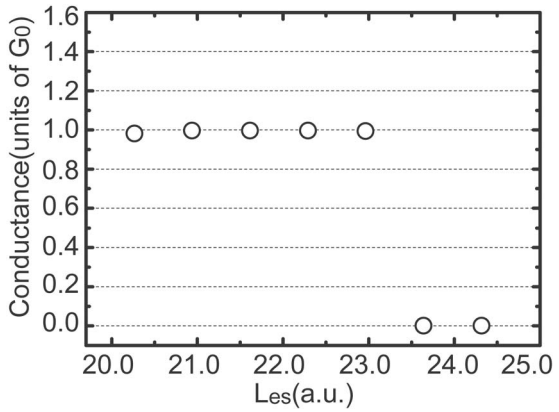

FIG. 6. Conductance of optimized three-sodium-atom nanowire in the unit of $G_0(=2e^2/h)$ as a function of electrode spacing.

expression for the conductance G at the zero-bias limit is given by the Landauer-Büttiker formula [34],

$$G = \frac{2e^2}{h} \sum_{i,j} T_{ij}(E_F), \tag{15}$$

which is given by the quantum-mechanical transmission probability T_{ij} of the incident electrons. Because only the electrons with the Fermi energy E_F contribute to the conductance of the zero-bias limit, we are only interested in $T_{ij}(E_F)$. Figure 6 shows the conductance versus the electrode spacing. The conductance is found to be close to 1 G_0 and insensitive to the elongation of the wire, which is consistent with previous experimental and theoretical results regarding the sodium nanowire [5,26,27,35–37]. Therefore, we are assured that the accuracy and efficiency of our procedure for the semi-infinite system.

IV. CONCLUSION

We have presented an efficient first-principles calculation method to treat a nanostructure between semi-infinite crystalline bulks by means of the RSFD method incorporating the localized orbital technique. Using the direct minimization of the MGC energy functional, we can obtain the self-consistent ground-state electronic structure as the mathematically well-defined minimum of the energy functional. The present method enables us to implement highly accurate calculations of the self-consistent electronic structures of almost any semi-infinite system. As numerical examples, we demonstrated the electronic structure calculations of a one-dimensional system and of single-row Na nanowires sandwiched between crystalline bulks. The calculated electronic structure for the one-dimensional system agreed with the exact analytical solution. As for the Na nanowire, the electron-charge distribution of the transition region matched those of the bulk regions across the boundaries between the transition region and the bulk region, and the electron-conduction properties are consistent with those obtained by experimental and theoretical studies [5,26,27,35–37]. In addition, the computational effort is proportional to the number of atoms N,

which is favorable in comparison with the Green's function methods. We can thus conclude that our procedure is suitable for the self-consistent electronic structure calculations of nanostructures suspended between semi-infinite crystalline bulks.

There is the possibility for the further development of our procedure. The direct minimization procedure employed here enables us to implement large-scale simulations with linear system-size scaling for studies on the structural properties of semi-infinite systems, e.g., the oxidation of surfaces. In addition, the localized orbital technique can accelerate the calculations of conduction properties using the overbridging boundary-matching method. We will discuss these developments in future publications.

ACKNOWLEDGMENTS

This research was partially supported by a Grant-in-Aid for the 21st Century COE "Center for Atomistic Fabrication Technology," a Grant-in-Aid for Scientific Research in Priority Areas "Development of New Quantum Simulators and Quantum Design" (Grant No. 17064012), and a Grant-in-Aid for Young Scientists (B) (Grant No. 18760031) from the Ministry of Education, Culture, Sports, Science and Technology. The numerical calculations were carried out using the computer facilities at the Institute for Solid State Physics at the University of Tokyo and the Information Synergy Center at Tohoku University.

[1] *Molecular Electronics: Science and Technology*, edited by A. Aviram and M. A. Ratner (New York Academy of Sciences, New York, 1998), and references therein.
[2] J. M. van Ruitenbeek, *Metal Clusters at Surface Structure, Quantum Properties, Physical Chemistry* (Springer, New York, 2000), and references therein.
[3] P. Hohenberg and W. Kohn, Phys. Rev. **136**, B864 (1964).
[4] N. D. Lang, Phys. Rev. B **52**, 5335 (1995).
[5] S. Tsukamoto and K. Hirose, Phys. Rev. B **66**, 161402(R) (2002).
[6] Y. Liu and H. Guo, Phys. Rev. B **69**, 115401 (2004).
[7] W. Press, B. P. Flannery, S. A. Teukolsky, and W. T. Vettering, *Numerical Recipes* (Cambridge Univ. Press, Cambridge, England, 1989).
[8] J. R. Chelikowsky, N. Troullier, and Y. Saad, Phys. Rev. Lett. **72**, 1240 (1994).
[9] J. R. Chelikowsky, N. Troullier, K. Wu, and Y. Saad, Phys. Rev. B **50**, 11355 (1994).
[10] T. Ono and K. Hirose, Phys. Rev. Lett. **82**, 5016 (1999).
[11] T. Ono and K. Hirose, Phys. Rev. B **72**, 085115 (2005).
[12] T. L. Beck, Rev. Mod. Phys. **72**, 1041 (2000).
[13] K. Hirose, T. Ono, Y. Fujimoto, and S. Tsukamoto, *First-Principles Calculations in Real-Space Formalism* (Imperial Colleage Press, London, 2005).
[14] J.-L. Fattebert and J. Bernholc, Phys. Rev. B **62**, 1713 (2000).
[15] G. F. Bertsch, J.-I. Iwata, A. Rubio, and K. Yabana, Phys. Rev. B **62**, 7998 (2000).
[16] T. Hoshi, M. Arai, and T. Fujiwara, Phys. Rev. B **52**, R5459 (1995).
[17] K. Hirose and T. Ono, Phys. Rev. B **64**, 085105 (2001).
[18] F. Mauri, G. Galli, and R. Car, Phys. Rev. B **47**, 9973 (1993).
[19] J. Kim, F. Mauri, and G. Galli, Phys. Rev. B **52**, 1640 (1995).
[20] R. L. Kronig and W. G. Penney, Proc. R. Soc. London, Ser. A **130**, 499 (1930).
[21] C. Kittel, *Introduction to Solid State Physics*, 8th ed. (Wiley, New York, 2004).
[22] N. Agraït, G. Rubio, and S. Vieira, Phys. Rev. Lett. **74**, 3995 (1995).
[23] J. C. Cuevas, A. Levy Yeyati, A. Martín-Rodero, G. R. Bollinger, C. Untiedt, and N. Agraït, Phys. Rev. Lett. **81**, 2990 (1998).
[24] J. M. Krans, C. J. Muller, I. K. Yanson, T. C. M. Govaert, R. Hesper, and J. M. van Ruitenbeek, Phys. Rev. B **48**, 14721 (1993).
[25] A. I. Yanson and J. M. van Ruitenbeek, Phys. Rev. Lett. **79**, 2157 (1997).
[26] J. M. Krans, J. M. van Ruitenbeek, V. V. Firsun, I. K. Yanson, and L. J. de Jongh, Nature (London) **375**, 767 (1995).
[27] J. M. Krans, J. M. V. Ruitenbeek, and L. J. D. Jongh, Physica B **218**, 228 (1996).
[28] J. P. Perdew and A. Zunger, Phys. Rev. B **23**, 5048 (1981).
[29] N. Troullier and J. L. Martins, Phys. Rev. B **43**, 1993 (1991).
[30] See K. Kobayashi, Comput. Mater. Sci. **14**, 72 (1999).
[31] D. R. Hamann, M. Schluter, and C. Chiang, Phys. Rev. Lett. **43**, 1494 (1979).
[32] We have tested that the enlargement of the size of localized orbitals does not change significantly the results obtained.
[33] Y. Fujimoto and K. Hirose, Phys. Rev. B **67**, 195315 (2003).
[34] M. Büttiker, Y. Imry, R. Landauer, and S. Pinhas, Phys. Rev. B **31**, 6207 (1985).
[35] Y. J. Lee, M. Brandbyge, M. J. Puska, J. Taylor, K. Stokbro, and R. M. Nieminen, Phys. Rev. B **69**, 125409 (2004).
[36] P. A. Khomyakov and G. Brocks, Phys. Rev. B **70**, 195402 (2004).
[37] Y. Egami, T. Ono, and K. Hirose, Phys. Rev. B **72**, 125318 (2005).